Volume 9 | Number 4 | April 2017 | Pages 337–426

Metallomics

rsc.li/metallomics

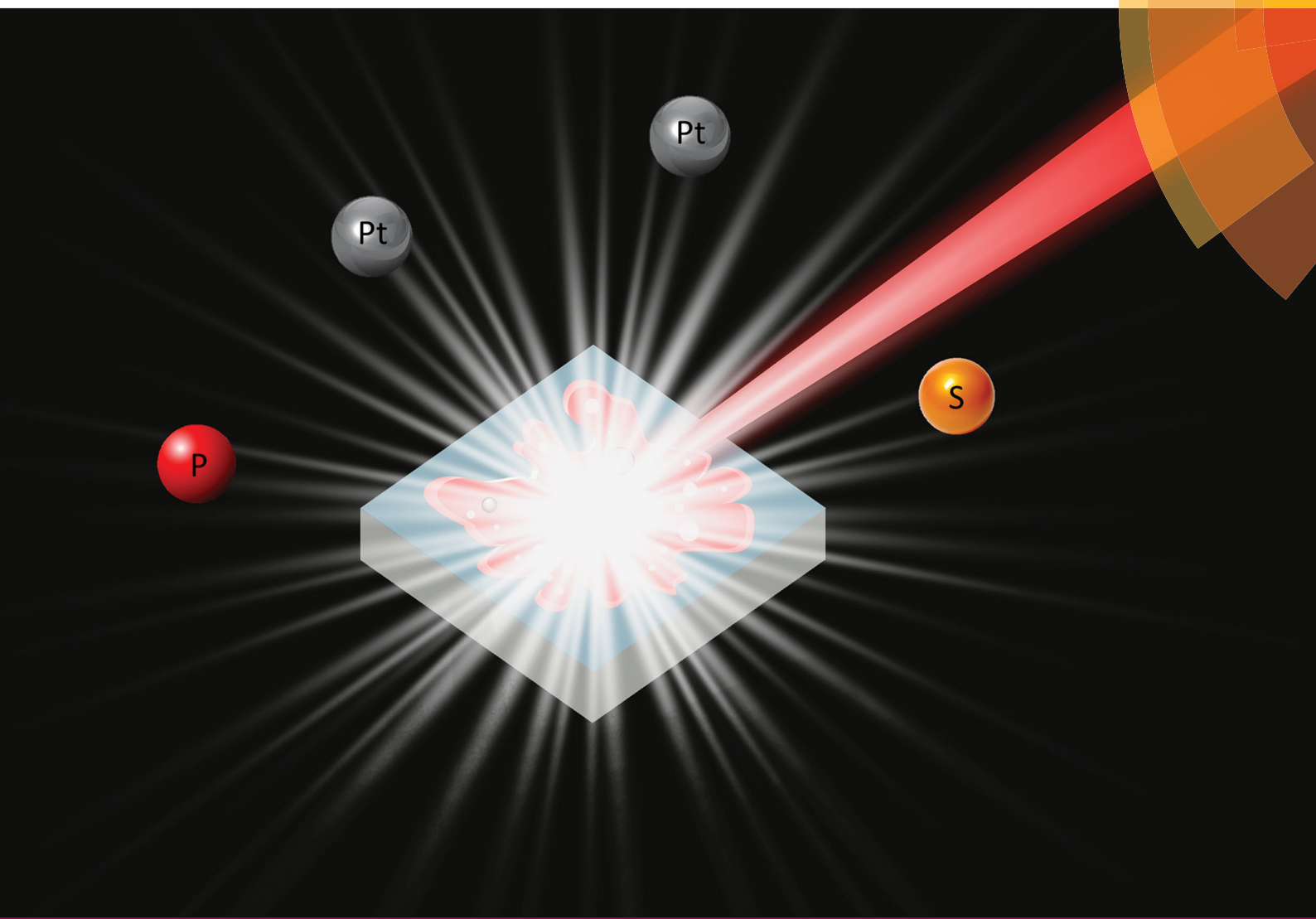

Themed issue: Imaging Metals in Biology

ISSN 1756-591X

ROYAL SOCIETY OF CHEMISTRY

TUTORIAL REVIEW
Paul J. Dyson *et al.*
Application of imaging mass spectrometry approaches to facilitate metal-based anticancer drug research

Metallomics

TUTORIAL REVIEW

View Article Online
View Journal | View Issue

Cite this: *Metallomics*, 2017, 9, 365

Application of imaging mass spectrometry approaches to facilitate metal-based anticancer drug research

Ronald F. S. Lee,†[a] Sarah Theiner,†[b] Anders Meibom,[cd] Gunda Koellensperger,[b] Bernhard K. Keppler[ef] and Paul J. Dyson*[a]

Received 10th October 2016,
Accepted 20th January 2017

DOI: 10.1039/c6mt00231e

rsc.li/metallomics

Mass spectrometry imaging is being increasingly used in metal-based anticancer drug development to study elemental and/or molecular drug distributions in different biological systems. The main analytical tools employed are SIMS (especially nanoSIMS), LA-ICP-MSI and MALDI-MSI as well as a combination of complementary imaging techniques. Main challenges are appropriate sample preparation methods, reliable and validated quantification strategies and a trade-off between sensitivity and spatial resolution. So far, research has mostly focused on the development of analytical methods for imaging with the long term goal to study drug uptake into tumor tissue and toxicity affected organs and to identify cellular targets of metal-based drugs. In this review we cover the technological features of the mass spectrometry imaging methods used and give an overview of the applications in metal-based anticancer drug research as well as some future perspectives.

Introduction

Since the discovery of the anti-tumor properties of cisplatin by Rosenberg in 1965,[1] metallodrugs have played an important role in cancer treatment. Today, platinum(II) drugs such as cisplatin, carboplatin, and oxaliplatin are used in more than 50% of all cancer chemotherapy regimens.[2,3] Advanced-stage development of various platinum(II) and platinum(IV) complexes are currently in different phases of clinical trials.[3] In addition, there are several non-platinum metal complexes also in clinical development[4] including two ruthenium(III) complexes, imidazolium *trans*-[tetrachloro(dimethyl sulfoxide) (imidazole)ruthenate(III)], NAMI-A, and indazolium/sodium *trans*-[tetrachlorobis(1*H*-indazole)-ruthenate(III)], KP1019/KP1339.[5–8] While extensive studies to develop new platinum- and ruthenium-based drugs continue, compounds based on other metals including rhenium, rhodium iron, gold, iridium and osmium are also being considered for their anti-cancer properties.[4,9,10]

A key aspect of metal-based anticancer drug research involves the study of how these drugs distribute within organs, tissues and cells. This is important because the distribution of a metallodrug within tissues and cells is linked with its effectiveness, its toxicity to healthy tissues and associated side effects, as well as drug resistance. The efficacy of, and resistance to, metallodrugs with the same metal center, for example cisplatin and oxaliplatin (both platinum(II)-based complexes) can differ dramatically: cisplatin is primarily used to treat testicular, ovarian, and lung cancers,[11] whereas oxaliplatin is used to treat colorectal cancers.[12] Furthermore, these two compounds also have different side effect profiles, *i.e.* cisplatin leads to nephrotoxicity whereas oxaliplatin generally causes peripheral neuropathy.[13] Similar to platinum-based drugs, the profile of the anti-tumor effect of drugs based on ruthenium strongly depends on their ligands, which can be chosen to yield either a high activity to primary cancers, such as the complexes NKP1339[7] and RM-175,[8] or anti-metastatic and anti-angiogenic properties, as observed, *e.g.* for NAMI-A and RAPTA-T.[7,8,14] The ligands confer different physicochemical properties to the drug and, in turn, lead to differences in the intra-cellular distribution, resulting in different pharmaceutical effects. It should also be noted that most metal-based anticancer drugs currently clinically applied or under development are actually pro-drugs, which become activated by oxidation state changes, *e.g.* platinum(IV) to platinum(II) and

[a] *Institute of Chemical Sciences and Engineering, École Polytechnique Fédérale de Lausanne (EPFL), CH1-1015 Lausanne, Switzerland. E-mail: paul.dyson@epfl.ch*
[b] *Institute of Analytical Chemistry, University of Vienna, Währinger Straße 38, 1090 Vienna, Austria*
[c] *Laboratory for Biological Geochemistry, School of Architecture, Civil and Environmental Engineering (ENAC), École Polytechnique Fédérale de Lausanne (EPFL), CH-1015 Lausanne, Switzerland*
[d] *Center for Advanced Surface Analysis, Institute of Earth Sciences, University of Lausanne, CH-1015 Lausanne, Switzerland*
[e] *Institute of Inorganic Chemistry, University of Vienna, Währinger Straße 42, 1090 Vienna, Austria*
[f] *Research Platform 'Translational Cancer Therapy Research', University of Vienna, Währinger Strasse 42, 1090 Vienna, Austria*
† These authors contributed equally to this paper.

ruthenium(III) to ruthenium(II),[6] or ligand exchange processes, such as hydrolysis of platinum(II)[15] and ruthenium(II) complexes.[16] Thus, it is possible that ligands initially coordinated to the metal center have a biological fate different from the metal ion once the drug enters the organism. For these reasons, it would be highly advantageous to be able to image the distribution of these compounds and, ideally, be able to distinguish between the metal and ligands, at the tissue and cellular level in biological systems. An ideal imaging technique would be able to image the distribution of the metal center, provide information about its oxidation state, and simultaneously map the distribution of the associated ligands with high sensitivity and spatial (*i.e.* subcellular) resolution. Moreover, there should be no modification of the parent drug so that it can be applied to live biological matter without a risk of modifying the biological behavior of the compound. In the literature, various imaging methods have been explored, such as classical and super resolution fluorescence microscopy,[17–20] synchrotron radiation induced X-ray fluorescence,[21,22] classical electron microscopy[23] and its more advanced applications such as energy filtered transmission electron microscopy (EFTEM)[22] and mass spectrometry imaging (MSI).[24–27] A number of excellent overviews of these methods in metallomics research are available.[28,29] Amongst these imaging techniques, MSI is particularly attractive as it meets many of the desirable qualities required for imaging metallodrugs in biological systems. First, MSI measures accurately either the mass of the entire compound or of individual elements or isotopic composition that identifies the compound. Second, MSI generally requires little (if any) modifications to the structure or composition of the parent compound; stable isotopic labels that do not alter the physicochemical properties of the parent compound can be employed. Third, different MSI modalities each possess specific and complementary strengths. For example, the high spatial resolution of NanoSIMS or the high sensitivity and raster rate of LA-ICP-MSI. However, a drawback of MSI techniques is the lack of information on the oxidation state of metals, which is essential for understanding intracellular activation, activity, and possible elimination of metallodrugs.

In recent years there have been significant advancements in MSI for metallomics applications, especially for NanoSIMS and LA-ICP-MSI. In this review, we describe the latest technological developments and applications in MSI relevant to metal-based anticancer drug research, the instrumentation involved, and provide a discussion of the advantages and limitations of the available techniques. We then explore the latest developments and applications of MSI for imaging cells, tissues, and organs.

Studying the distribution of metallodrugs in biological systems

The principal MSI techniques for detecting and imaging metallodrugs are matrix assisted laser desorption ionization-mass spectrometry imaging (MALDI-MSI), laser ablation-inductively coupled plasma mass spectrometry imaging (LA-ICP-MSI), secondary ion mass spectrometry (SIMS) techniques, including nanoscale ion microprobe SIMS (NanoSIMS), and time-of-flight SIMS (TOF-SIMS). An overview and comparison of the analytical features, advantages and limitations of these mass spectrometry-based imaging techniques is provided in Fig. 1 and Table 1. In general, all MSI methods involve the rastering of a primary laser or ion beam onto a sample surface generating ions that are subsequently detected using a mass spectrometer. Images of single m/z ions are then generated with the relative abundance displayed as a false color image (in which colors represent signal intensity in each signal). MSI does not require modification of the parent compound for detection. However, isotopic labeling can be applied in certain cases either to increase the signal of endogenously ubiquitous elements or for quantitation.

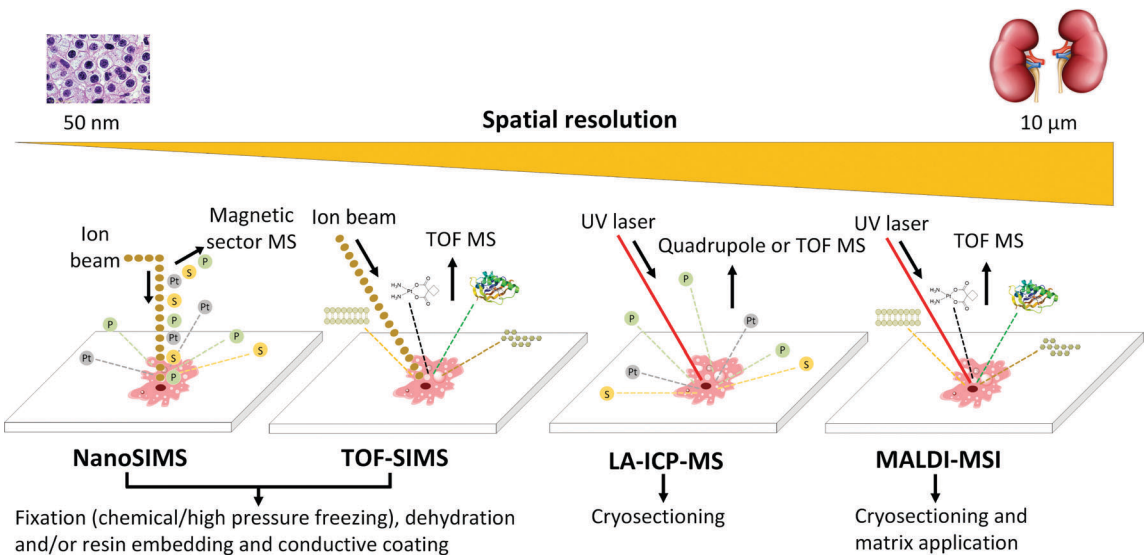

Fig. 1 Illustration of the ionization sources of the different MSI techniques employed in the study of metal-based drugs.

Table 1 Comparison of different imaging techniques applied to the study of metal-based anticancer drugs

Technique	Relative ionization strength	Spatial resolution	Analyte type	Advantages	Disadvantages	Metal drug elements imaged
Nano-SIMS	Hard	Down to 50 nm	Atoms	High spatial resolution High sensitivity for smaller elements	Low sensitivity for transition metals Small sampling area Sample preparation must resist high vacuum Samples must be flat	Pt, Ru, Au
LA-ICP-MSI	Hard	Down to 1 μm	Atoms	High sensitivity for transition metals Operates at atmospheric pressures	Low spatial resolution	Pt, Ru
MALDI-MSI	Soft	Down to 1 μm	Molecules	Analysis of full *m*/*z* range Can operate at atmospheric pressures Non destructive	Samples must be covered in an organic matrix Low spatial resolution	Pt
TOF-SIMS	Hard	Down to 100 nm	Molecules	Can analyse molecules Analyses a full range of *m*/*z*	Low sensitivity for transition metals Small sampling area Sample preparation must resist high vacuum Samples must be flat	Pt

Imaging with secondary ion mass spectrometry

SIMS is a surface MSI technique in which a solid sample surface is evaporated under high vacuum conditions through sputtering by a primary ion beam. A positive ion beam (*e.g.* Ga^+, Cs^+, Bi^+ and Ar^+) is used to generate negative secondary ions and a negative ion beam (*e.g.* O^-) to generate positive secondary ions.[30,31] SIMS instruments are equipped with a time of flight mass analyzer (TOF-SIMS) or a magnetic sector field mass analyzer (NanoSIMS). Signal intensities are dependent on the product of the sputter yield and the ionization probability, which can vary over several orders of magnitude. The high spatial resolution (~50–100 nm) allows NanoSIMS to be applied to the determination of cellular distributions of metallodrugs and, simultaneously, the organic ligands associated with the metal center. However, ligands can only be visualized by NanoSIMS if they possess non-endogenously ubiquitous elements in their chemical structure (*e.g.* Br, F) or have been isotopically labelled (*e.g.* ^{13}C, ^{15}N). For metal detection *via* NanoSIMS it should be noted that, in general, semi-thin sections must be used due to the relatively high beam strengths and long acquisition times (>10 hours) required to obtain sufficient secondary ion yields, conditions that would typically destroy a thin section.[32]

SIMS instruments integrated with TOF mass spectrometry allow very sensitive detection of elements ranging from 0–10 000 Da, with a spatial resolution of about 100 nm. In practice, achieving such a spatial resolution is challenging as focusing a narrow primary ion beam leads to a tradeoff between sensitivity and mass resolution.[33] Thus, a compromise between these parameters must be found. A good example illustrating this point is the TOF-SIMS imaging of cisplatin in glioblastoma cells which was performed with a spatial resolution of 500 nm, mass range detection of 1–1000 Da, and sufficient sensitivity to detect platinum.[34]

A critical step for (Nano)SIMS concerns the sample preparation. The analysis is performed under ultra-high vacuum conditions and both the structural and chemical integrity of cells and tissue have to be preserved. Sample preparation strategies are explained in detail elsewhere.[32] Often, biological samples for SIMS are prepared in a similar manner to those for electron microscopy.[35] Samples are usually fixed either chemically or *via* high pressure freezing (HPF), then dehydrated/freeze substituted and finally infiltrated with a resin. It is assumed that freeze substitution helps to preserve the chemical integrity of a biological sample, as the fixation and dehydration happens in the cold and can potentially preserve the hydration shell.[36] However, the use of HPF is also challenging, as cell samples do not always freeze well and cryo-protective additives (such as sugars, polymers and proteins) are required, which can alter SIMS ion yields. Prior to analysis, resin-embedded samples must be cut into thin sections (~50 nm) or semi-thin sections (200–1000 nm), loaded onto TEM grids, silicon wafers, or glass slips, and finally gold-coated to increase the electrical conductivity of the sample surface.[32]

Imaging with laser ablation-inductively coupled plasma-mass spectrometry

Inductively coupled plasma-mass spectrometry (ICP-MS) is ideally suited to studying the fate of metallodrugs in biological systems due to low limits of detection (ppt to ppq range) for most metals and the possibility of online coupling to different separation techniques (*e.g.* HPLC or capillary electrophoresis).[37,38] It is routinely used to investigate the pharmacokinetics of metallodrugs by determining the total metal content in tissue samples and serum, as well as the cellular uptake of metallodrugs either in the whole cell or in different cellular compartments (*e.g.* nucleus, cytoplasma, mitochondria *etc.*) after separation.[37,39,40] However, samples are either digested or homogenized, leading to destruction of the structural integrity of the cells.

Coupling of a laser ablation system to ICP-MS provides the advantage of high spatial resolution (down to the cellular level) combined with the high sensitivity, wide concentration dynamic range and multielement analysis capabilities of the

ICP-MS detection system.[24,41,42] The sample preparation methods required for bioimaging with LA-ICP-MSI are straightforward compared to, for example, MALDI-MSI or SIMS imaging methods. Most LA-ICP-MSI studies rely on cryo-sections (with a thickness between 5 and 30 μm) to preserve the biological material and the elemental distributions in their native physiological conditions. As paraffin-embedding is a routine procedure for histopathological evaluations it is also widely employed in LA-ICP-MSI experiments. However, in this process samples undergo several washing steps and are fixed with formalin, which may potentially result in alteration of elemental concentrations and distributions.[27,43]

In LA-ICP-MSI, the sample material is ablated with a focused laser beam and the generated aerosol is transferred *via* a carrier gas to the ICP-MS system. Most commonly quadrupole mass analyzers are employed and for certain applications a magnetic sector field mass analyzer is used. With the introduction of ICP-TOF-MSI, pseudo-simultaneous measurement of a whole range of elements became feasible.[27,41] Solvent- or air-based interferences by oxygen or nitrogen are absent in LA-ICP-MSI simplifying the nature of the ions produced, although short integration times of the ICP-MS detection, required to account for the transient nature of the ablation signals, limit precision. A disadvantage of LA-ICP-MSI is the long acquisition time (several hours are required to obtain high-resolution images).[42] Recent developments in ablation cell design have significantly reduced the washout times and the pulse response duration of single laser shots resulting in lower acquisition times and higher spatial resolution.[44,45]

In comparison to MALDI-MSI and imaging by (Nano-)SIMS, quantification by LA-ICP-MSI is straightforward. For bioimaging by LA-ICP-MSI various concepts have been discussed in literature for the validation and reliable quantification of samples including the use of internal standards and different calibration methods.[46,47] Quantification is strongly matrix dependent and in bioimaging studies using LA-ICP-MSI, matrix-matched standards (homogenized liver, chicken breast, kidney, blood *etc.*) are most commonly employed.[46,48,49] As an alternative, polymer-, gelatine- and solution-based standards have been proposed. For internal standardization, elements are usually selected that are intrinsically present and homogenously distributed in the sample and the most commonly used isotope is ^{13}C.[50] Other approaches rely on the deposition of an internal standard layer under or on the surface of the tissue, *e.g.* spin-coated elemental or gold sputtered internal standards, with the requirement of simultaneous ablation of both layers.[51–53] Every concept has its advantages and drawbacks and, ideally, the development of quantification strategies for every analytical problem and sample material is optimal.

Matrix assisted laser desorption ionization-imaging mass spectrometry

Biological samples for MALDI-based MSI are embedded in a matrix containing a chromophore after which a UV laser beam is rastered over the sample surface causing photo-volatilization and ionization of the sample which is then transferred to a mass analyser.[54] MALDI-MSI employ either TOF or Fourier transform ion cyclotron resonance (FT-ICR) mass analysers and the analysis can be performed under atmospheric pressure conditions.[55] The type of mass analyser used depends on the application, with TOF instruments allowing macromolecules of even 100 kDa to be detected, whereas FT-ICR provides high resolution analysis, but generally with a much lower mass range.[55] The spatial resolution is currently limited by factors such as the laser focal diameter, matrix crystal size/homogeneity, and displacement of analytes during matrix deposition.[25] Nevertheless, recent advances in both instrument performance and matrix deposition methods allow a spatial resolution of ~1–10 μm to be achieved.[55,56] With this comparative low resolution MALDI-MSI is currently more useful for tissue/organ level analysis than for imaging at the cellular level. The choice of matrix is also critical for metallodrug analysis as certain matrices can decrease ionization efficiency and lead to lower detection sensitivity.[57]

Applications of MSI in metal-based anticancer drug development

An overview of the application of MSI studies to the vizualisation of metal-based anticancer drugs in biological samples is given in Table 2. Most of the studies focus on the development of analytical setups to obtain insights into the mode of action of metallodrugs at a cellular level. This includes elucidating possible targets of metallodrugs inside the cell, the study of drug tumor penetration/tumor response to drug treatment and therapy-related side effects and toxicity.

MSI for cellular imaging of metallodrugs

Imaging metallodrugs in cells requires high spatial resolution in order to resolve cellular structures and organelles. Consequently, NanoSIMS is the MSI technique most widely used to probe the cellular distribution of metallodrugs, as it can achieve spatial resolutions of 50–100 nm for metals and it can be used in conjunction with fluorescence microscopy,[61] or electron microscopy,[59] to further resolve cellular structures. SIMS methods have been used to characterize the cellular distribution of several metallodrugs based on gold, platinum and ruthenium to elucidate their cellular targets and possible mode of action.[60–63]

Platinum complexes act largely in the nucleus of cells, forming adducts with DNA leading to cell apoptosis.[18] The first reported use of NanoSIMS was to study cisplatin-induced intracellular alterations to the composition of kidney (LLC-PK_1) cells treated with 6 μM cisplatin for 4 hours.[64] Although intracellular Pt was detected, subcellular distributions could not be discerned due to the low spatial resolution (500 nm) of the experiment. Nevertheless, this study showed the potential of NanoSIMS to study the distribution of metallodrugs at a cellular level and identified the major challenge, which is the low sensitivity for certain transition metals.[64] Subsequently, the cellular distribution of the two ^{15}N labelled platinum(II) complexes, cisplatin and TriplatinNC (Fig. 2), was determined in MCF7 human breast adenocarcinoma cells dosed at 20 μM

Table 2 Applications of mass spectrometry imaging techniques in metal-based anticancer drug research

NanoSIMS and TOF-SIMS

Metallodrug	Tissue type/cell line	Spatial resolution	Analytes	Fixation method	Reference
Oxaliplatin	HeLa cells	—	$^{12}C^{14}N$, $^{12}C^{15}N$ ^{195}Pt	Chemical fixation	58
Pt(IV) complexes	Kidney, CT-26 tumor	80 nm	$^{12}C^{14}N$, ^{31}P, ^{34}S, ^{195}Pt	Chemical fixation	59
RAPTA-T	A2780CR cells	—	$^{12}C^{14}N$, $^{12}C^{15}N$, ^{31}P, ^{32}S, ^{102}Ru	Chemical fixation	60
Cisplatin	Glioblastoma cells	500 nm		Chemical fixation	34
Cisplatin	SW480 cells	—	$^{12}C^{14}N$, ^{31}P, ^{34}S, ^{194}Pt	Chemical fixation	61
Cisplatin, triplatinNC	MCF7 cells	—	$^{12}C^{14}N$, ^{31}P, $^{12}C^{15}N$, ^{195}Pt	Cryo fixation	62
$[Au(d2pype)_2]Cl$	MDA-MB-231 cells	—	$^{12}C^{14}N$, ^{31}P, ^{34}S, ^{197}Au	Chemical fixation	63
Cisplatin	Renal epithelial cells	500 nm	^{195}Pt	Cryo fixation	64

MALDI-MSI and LA-ICP-MSI

Metallodrug	Tissue type/sample material	Spatial resolution	Analytes	Calibration standards	Reference
Cisplatin, carboplatin, oxaliplatin	Tumor spheroids	—	Oxaliplatin, Pt(dach)methionine	None	65
Cisplatin, oxaliplatin	Tumor	—	Oxaliplatin, Pt(dach)methionine	None	57
Oxaliplatin	Kidney	—	Oxaliplatin, Pt(dach)methionine, Pt(dach)cysteine	None	66
Cisplatin	Gel electrophoresis	—	Pt	None	67
Cisplatin, NAMI-A	Gel electrophoresis	—	Pt, Ru	None	68
Cisplatin	Gel electrophoresis	—	Pt	None	69
Cisplatin	Monkey kidney	~1 μm	Pt	Gelatin standards	70
Cisplatin, Pt(II) complexes	Mouse liver, kidney	50 μm	Pt	None	71
Cisplatin	Human tumor	40 μm	P, Fe, Cu, Zn, Pt	None	72
Pt(IV) complexes	Tumor, tumor spheroids	70 μm	Pt	Matrix-matched liver standards	73
Pt(IV) complexes	Tumor spheroids	10 μm	Pt	None	74
KP1019, NAMI-A	Tumor spheroids	10 μm	Ru	None	75
Cisplatin	Tumor spheroids	5 μm	Pt	Matrix-matched standards	76
Pt(IV) complexes	Tumor, kidney	70 μm	Pt	Matrix-matched liver standards	59
Cisplatin, carboplatin, oxaliplatin	Kidney	100 μm	Pt, Cu, Zn	None	77
Cisplatin	*Caenorhabditis elegans*	5 μm	Pt	None	78
Cisplatin	Testis, cochlea, kidney, nerve, brain	14 μm	Pt	Polymer-based standards	79
Oxaliplatin, satraplatin, Pt(IV) complexes	Tumor, kidney	70 μm	Pt	Matrix-matched liver standards	80
Cisplatin, oxaliplatin	Muscle, nerve, connective, fat tissue	70 μm	Pt	Matrix-matched liver standards	81
Cisplatin, NKP1339	Kidney, liver, spleen, muscle	70 μm	Pt, Ru	Matrix-matched liver standards	48
Cisplatin, oxaliplatin	Tumor	200 μm	Pt	None	57
Cisplatin	Kidney, cochlea, testis	50 μm	Pt	Polymer-based standards	82
Cisplatin	Kidney	25 μm	Pt	None	83
Oxaliplatin	Tumor	70 μm	Pt	Gelatin standards	84
Cisplatin	Kidney	8 μm	Pt, Zn, Cu	Matrix-matched kidney standards	85
Cisplatin	Hair	300 μm	Pt	Matrix-matched hair standards	86
Cisplatin	Kidney	50 μm	Pt, Zn, Cu	Matrix-matched standards	87

for 1 or 2 hour incubation periods. The images showed that the polynuclear platinum compound, TriplatinNC, accumulated in the nucleolus and in cytoplasmic vesicle-like structures. Interestingly, an increased non-correlation between ^{15}N and Pt signals was observed at the longer incubation time, indicating that the NH_3 ligands dissociate from the platinum complex.[62]

A more recent study combined fluorescence microscopy with NanoSIMS analysis to map the distribution of cisplatin in SW480 colorectal cancer cells.[61] Cells were treated with ^{15}N labelled cisplatin (at different concentrations ranging from 0–150 μM for 24 hours) and Pt was found to accumulate in small cytoplasmic sulfur-rich aggregates, acidic organelles and the nuclei. From plots of ^{15}N *vs.* Pt accumulation in different cellular organelles, a partial dissociation of the Pt–N bonds seems likely, particularly within the nucleolus at high cisplatin concentrations (*ca.* 150 μM). With correlative fluorescence microscopy using lysotracker red to label acidic organelles, overlapped Pt and fluorescence images showing accumulation of cisplatin in these organelles.[61]

The distribution of cisplatin in U87MG human glioblastoma cells has been determined using TOF-SIMS in cells dosed with 30 μM of the compound for 48 hours.[34] Platinum concentrations were found to be up to 1.5 times higher in the nucleus compared to the cytoplasm. In addition, up to 40 different phospholipids were identified on the cell membrane, highlighting a key strength of TOF-SIMS through which, besides localization of the metallodrug, information on the surrounding cellular environment can be obtained simultaneously. However, current limitations in the spatial resolution for Pt detection in TOF-SIMS precluded

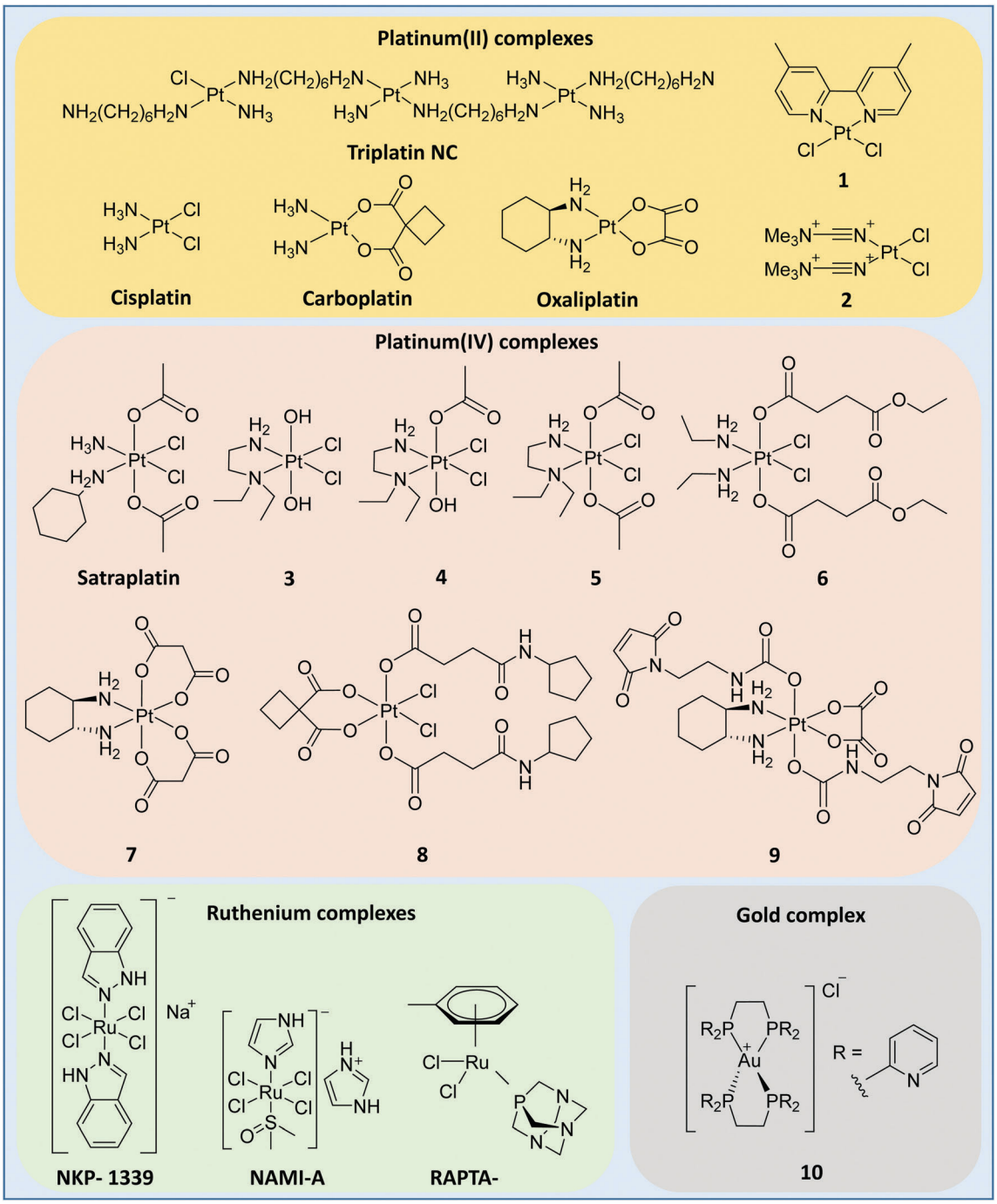

Fig. 2 Metal-based anticancer complexes mentioned in this review.

subcellular differentiation other than between the nucleus and cytoplasm.[34]

Platinum drug loaded nanoparticle formulations can help to target the drug to tumors, thereby potentially reducing side effects.[88] Probing the intracellular distribution of such nanomedicines is important to understand release characteristics of the metallodrug from the nanocarrier. In a recent study, the fate of oxaliplatin loaded in polymeric nanoparticles was studied in HeLa cells following treatment with 3 μM for 4 or 24 hours. Fluorescence structured illumination microscopy and NanoSIMS were combined to image the cellular distribution of the ^{15}N and fluorescent labelled nanoparticle polymer and oxaliplatin.[20] Fig. 3 shows NanoSIMS maps of nanoparticle treated cells at different times during the incubation. It can be seen that from 4 to 24 hour incubations, there is an increased uptake of the nanoparticles and a dissociation of ^{15}N from Pt signals showing the release of free Pt from the nanoparticle, which correlates well with the observed cytotoxicity of the formulation.

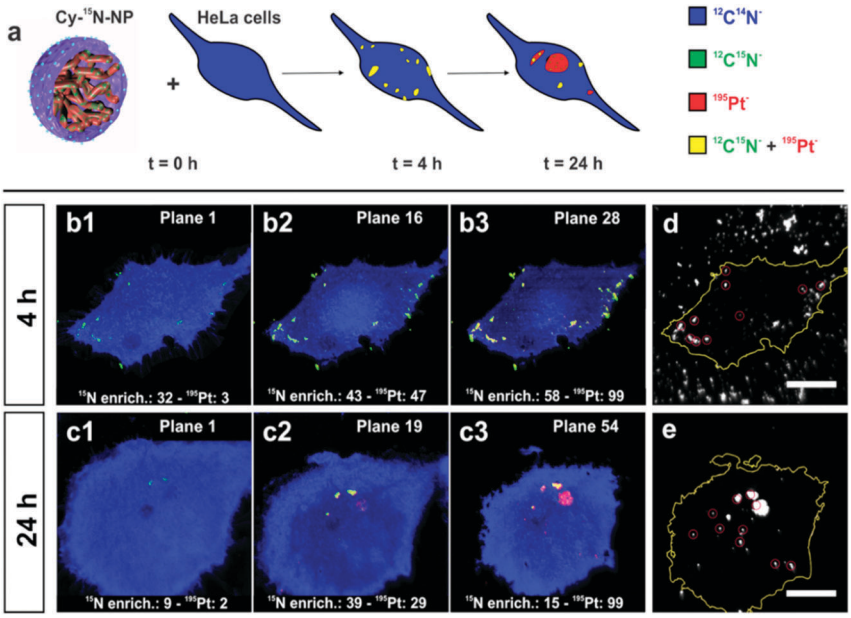

Fig. 3 (a) Scheme summarizing the time-dependent NanoSIMS experiments carried out in HeLa cells treated with Cy-^{15}N-nanoparticles. (b and c) HeLa cells incubated with Cy-^{15}N-nanoparticles for 4 h (top three panels, b1–b3) or 24 h (bottom three panels, c1–c3) and imaged by NanoSIMS. Removal of layers of organic matter from the cell surface followed by imaging shows co-localization (yellow) of the ^{195}Pt (red) and ^{15}N (green) of the nanoparticles inside the cell. The cell surface is represented by the $^{12}C^{14}N^-$ ion map (blue). Summed observed ^{195}Pt signals (white pixels) in HeLa cells incubated for 4 h (d) and 24 h (e). Red circles are the ROIs selected for $^{15}N/^{14}N$ quantification where ^{195}Pt counts are observed. Cell boundaries (yellow line) were delimited from the corresponding $^{12}C^{14}N^-$ ion images. The averaged ^{15}N and ^{195}Pt signals per selected ROIs at each of the selected planes are shown for panels b and c. The scale bars represent 10 μm (adapted with permission from ref. 58. Copyright 2016 American Chemical Society).

The distribution of two investigational platinum(IV) complexes (Fig. 2, complexes **6** and **9**) in tissues and cells extracted from an *in vivo* murine CT-26 colon cancer model was probed using LA-ICP-MSI and NanoSIMS.[59] LA-ICP-MSI was used to study the platinum accumulation on the tissue level in the kidney and tumor to select areas with highest Pt levels for further cellular distribution investigations using NanoSIMS. In the renal cortical cells Pt was found to accumulate in cells of the glomerulus relative to the tubules, with Pt concentrated in sulfur-rich organelles in the podocytes of the glomerulus. In tumor cells, similar amounts of platinum were detected in the nucleus and cytoplasm. However, Pt levels in the nucleolus were elevated and cytoplasmic Pt accumulation was also concentrated in sulfur-rich organelles, namely in lysosomes (identified by electron microscopy).[59]

Gold complexes are currently used in clinics as anti-arthritic medications and their potential as anticancer agents has also been investigated.[89–91] Gold has a high affinity towards organo-sulfur (S) and selenium (Se) moieties and it has been assumed that a subcellular target of certain gold complexes includes the thioredoxin system, a family of proteins responsible for redox homeostasis in the cytoplasm, mitochondria, and nucleus of cells.[92] Gold(I) complexes with bidentate phosphine ligands (Fig. 2, complex **10**) have been shown to be selectively toxic to cancer cells and therefore studying the cellular distribution of these complexes could help to confirm their mechanism of action.[89] In a combined study using NanoSIMS and energy filtered transmission electron microscopy (EF-TEM) the cellular distribution of the Au(I) phosphine complex, [Au(d2pype)$_2$]Cl, was investigated in MDA-MB-231 human breast adenocarcinoma cells.[63] Gold was observed to accumulate in aggregates, mostly in non-DNA containing nuclear areas and inside the nuclear membrane. Fig. 4 shows the elemental images of $^{31}P^-$, $^{197}Au^-$ and $^{34}S^-$, with overlaid images mapping Au and S rich regions. Images (c) and (d) in Fig. 4 show a clear co-localisation of Au and S which is in accordance with the hypothesis that gold complexes bind to S rich regions in the thioredoxin system.[63]

Some ruthenium-based metallodrugs, *e.g.* NAMI-A and RAPTA-T (Fig. 2), possess anti-metastatic and anti-angiogenic properties and therefore have a profoundly different mode of action to classical metallodrugs.[8,19,93–95] Studying the cellular distribution of this class of compounds could yield insights into the fate of metal ions in cells and might help to rationalise these specific properties. The cellular distribution of ^{15}N and ^{13}C labelled RAPTA-T was elucidated in the ovarian cancer cell line A2780 (cisplatin resistant).[60] A co-accumulation of ^{15}N and Ru was observed, but in the absence of ^{13}C, indicating that the phosphine ligand remains coordinated to the Ru ion, whereas the arene presumably dissociates to some extent. Indeed, arene loss from these complexes on binding to potential biomolecular targets has been demonstrated previously.[96,97] The Ru is distributed mainly in the cell membrane and interphase between cells, consistent with the observed anti-metastatic activity, which is partly mediated by extracellular matrix proteins.[60]

Metallodrug imaging at cellular level using LA-ICP-MSI

ICP-MS based approaches for analysis of metal-based drug uptake in cells usually determine average concentrations over a cell population by direct infusion. Information on the bulk

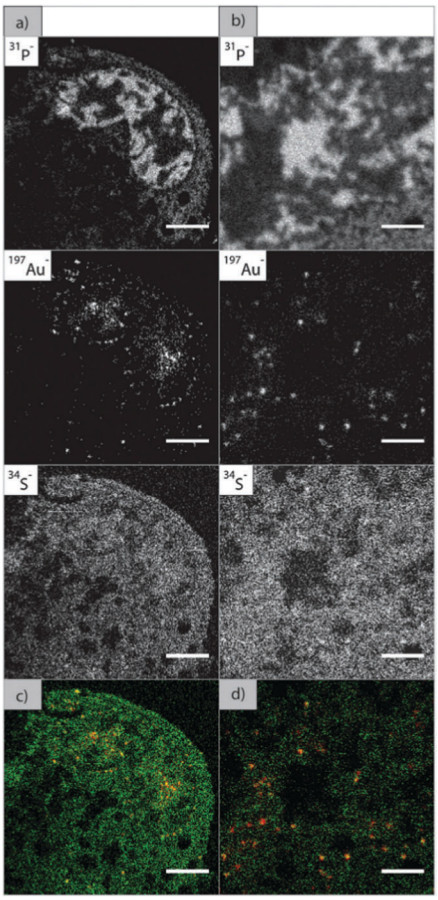

Fig. 4 (a and b) NanoSIMS ion maps showing ^{31}P and ^{197}Au and ^{34}S secondary ions in MDA-MB-231 cells after 2 h incubation with **10** (100 mM). (c and d) Are overlays of the ^{34}S and ^{197}Au ion maps shown in (a) and (b), respectively, where ^{34}S and ^{197}Au are falsely coloured in green and red, respectively. Yellow pixels indicate co-localisation of ^{34}S and ^{197}Au, which can be observed in the cytoplasmic, perinuclear and nuclear regions. Scale bars: (a) and (c) = 2 mm, (b) and (d) = 1 mm (adapted from ref. 63 with permission from the Royal Society of Chemistry).

concentration of single cells requires injecting single cells into the ICP-MS, using *e.g.* mass cytometry or micro-droplet generators.[98] For LA-ICP-MSI the spatial resolution is a function of the laser spot diameter, the number of sampling isotopes and the wash out times of the ablation cell.[45] Depending on the laser parameters used and the nature of the experiment the typical spatial resolution for bioimaging studies in tissue samples by LA-ICP-MSI lies between 5–100 μm.[27,41] In recent years, advances in ablation cell design as well as new sample preparation techniques (such as antibody or elemental labelling) and data processing have enabled the detection of elements with LA-ICP-MSI at the cellular level.[99,100] Thus far, the technique has been used to study, *e.g.* the distribution of biomarkers in breast cancer tissue with a spatial resolution of ~1 μm[99,101] and to study Ag and Au nanoparticles in cellular substructures of individual cells.[102] Recently, LA-ICP-MSI employing a low dispersion ablation cell and a data deconvolution approach has been used to determine Cu quantitatively in single cells of a model organism.[20] The same approach enabled to resolve the platinum distribution at (sub-)cellular level in kidney sections of monkeys after cisplatin treatment. Laterally resolved pixels of ~1 μm were achieved in regions of interest, where platinum was found to accumulate mainly in the renal cortical tubules, especially in the tubular epithelial cells.[70]

A recent study adapted a LA-ICP-MSI setup to determine the uptake of platinum(IV) complexes in multicellular tumor spheroids as a possible screening and selection tool for novel metallodrugs.[74] Three dimensional multicellular tumor models are increasingly used as bridge between conventional monolayer cell culture systems and animal models in preclinical metal-based anticancer drug development.[103–105] Depending on their size *in vitro* tumor spheroids are able to mimic the complex tumor microenvironment in terms of oxygen, pH gradients, the development of a necrotic core and hypoxic regions.[106,107] The spatial resolution of approximately 10 μm allowed the accumulation of platinum in the different compartments of the tumor spheroid to be visualized, showing that platinum(IV) complexes are not only taken up by the tumor spheroids, but are also able to penetrate into the different layers reaching the necrotic pseudo-tumor core (Fig. 5A).[74] In another study, Pt accumulation of cisplatin was investigated in TFK-1 tumor spheroids by LA-ICP-MSI with a spatial resolution of 5 μm. Different matrix-matched standards based on cell pellets, gelatine and egg yolk were evaluated to obtain quantitative data on Pt uptake. The highest Pt signal was observed in the proliferating zone with high cell density and cell division rate.[76]

The reduction behaviour of the ruthenium-based complexes KP1019 and NAMI-A (Fig. 2) has been studied in multicellular spheroids of SH-SY5Y human neuroblastoma cells.[75] The spheroids had different sizes to control hypoxia and to mimic normoxic, hypoxic, and necrotic environments (visualized by pimonidazole staining). A complementary approach based on LA-ICP-MSI and X-ray absorption near-edge spectroscopy (XANES) was employed to gain information on the ruthenium distribution and the oxidation state of the compounds. Single line scans by LA-ICP-MSI over different tumor spheroids confirmed penetration of KP1019 and NAMI-A into the spheroid hypoxic region. XANES analysis showed similar coordination environment of NAMI-A in spheroids of different degrees of hypoxia. For KP1019, in contrast, significant differences in Ru speciation in normoxic and hypoxic environments were observed pointing towards its reduction in the hypoxic tumor environment. These results are in accordance with the observation in clinical trials that KP1019 acts against primary tumors whereas NAMI-A shows anti-metastatic properties.[75]

MSI for imaging of metallodrugs at tissue level

LA-ICP-MS has emerged as the optimum tool to image the biodistribution of metallodrugs in biological samples. Initially, however, the first LA-ICP-MSI study involving metallodrugs was on the identification of the protein-binding partners of cisplatin. In this study, LA-ICP-MSI was used to analyze the platinum content of bacterial proteins upon treatment with cisplatin after separation with gel electrophoresis.[69] Subsequently, the protein-interactions of the investigational ruthenium complexes RAPTA-C[109,110] and NAMI-A[68] were studied, the latter in comparison

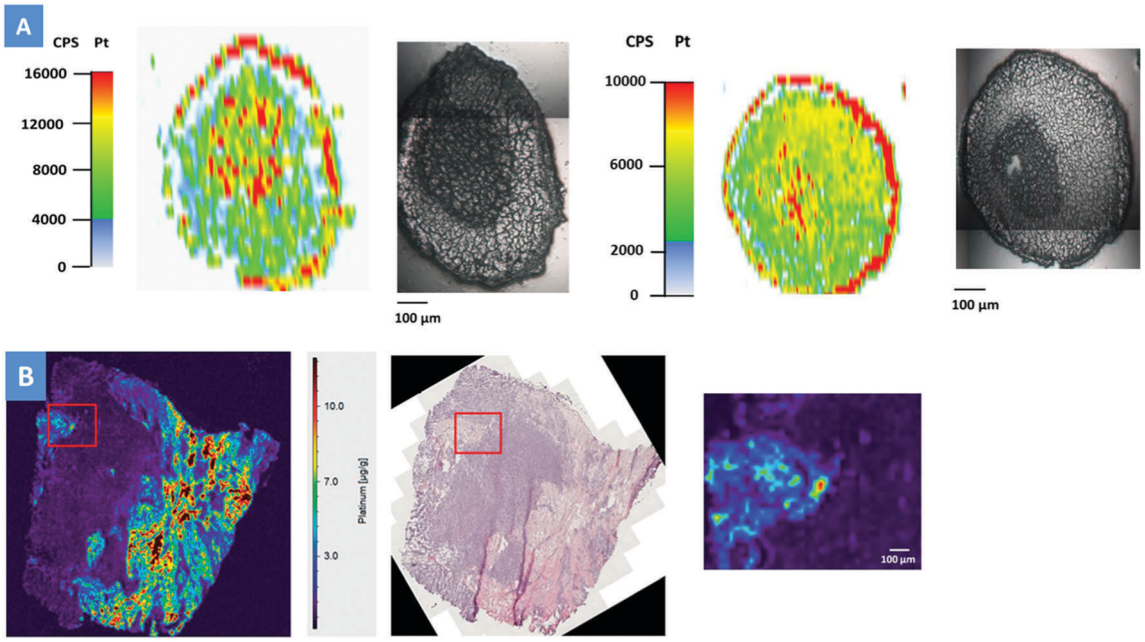

Fig. 5 (A) LA-ICP-MSI images of HCT116 and CH1 multicellular tumor spheroids after treatment with satraplatin (adapted from ref. 74 with permission from the Royal Society of Chemistry). (B) Human malignant pleural mesothelioma section, analyzed by LA-ICP-MSI and corresponding histological section (visualized by a haematoxylin and eosin stain). Magnification of an area of the tumor section (adapted from ref. 108 with permission from the Royal Society of Chemistry).

to cisplatin using native PAGE, SDS-PAGE and 2D gel electrophoresis followed by identification of the binding partners by LA-ICP-MSI combined with proteomics. LA-ICP-MSI has also been combined with nHPLC-ESI-LTQ-FT-MS/MS to study cisplatin–protein interactions after separation by 2D gel electrophoresis.[67] The advantage of these approaches over proteomics methods that do not permit detection of the metal drug,[23,110–113] is that the proteins highlighted are those to which the metallodrug is directly bound, rather than identifying up- and down-regulated protein expression levels. In practice, both approaches are complementary to understand how metallodrug-binding to proteins (and DNA) leads to changes in protein regulation and the observed pharmacological properties.

A promising application of MSI techniques within preclinical platforms is for the study of metal-based drug uptake in tumors. In the case of histologically heterogeneous structures, assessment of the spatial platinum accumulation pattern by LA-ICP-MSI was found to be advantageous compared to measurements of the total platinum content in tissues by ICP-MS.[80] The quantitative platinum distribution was determined by LA-ICP-MSI in an *in vivo* preclinical murine tumor model after administration of platinum(II)- and platinum(IV)-based complexes (Fig. 2; oxaliplatin, satraplatin, **6**, **7** and **8**). Higher platinum levels were detected in areas containing soft tissue, sparsely infiltrated with tumor cells compared to regions comprising densely packed tumor cells. The histologic features of the tumor tissue (visualized by a consecutive haematoxylin eosin stained slide) were reflected in the LA-ICP-MSI platinum distribution maps. For oxaliplatin, platinum enrichment correlated with areas of necrotic tissue.[80] In another study, direct infusion ICP-MS and a quantitative LA-ICP-MSI method were combined to investigate the bioavailability of oxaliplatin in rat tumor tissue. Different treatment schedules were compared including hyperthermic intraperitoneal chemotherapy (HIPEC), although from the accumulation studies this approach did not significantly increase oxaliplatin levels in tumors compared to normal thermal conditions.[84] A recent study investigated the distribution and penetration depth of Pt and biologically relevant elements (P, Mn, Ca, Zn, Fe, Br and S) in a murine ovarian xenograft model after intraperitoneal treatment with cisplatin (hyperthermic and normothermic treatment conditions). For this purpose, SR-XRF and LA-ICP-MSI were combined to study elemental distributions at nanoscopic and microscopic levels. Principle component analysis revealed a co-localisation of Pt with bromine and sulfur. A deeper Pt penetration (determined by SR-XRF) and higher Pt concentrations (determined by LA-ICP-MSI) were observed after hyperthermic cisplatin treatment. The Pt distribution in the tumor tissue was heterogeneous throughout the tumor with pronounced Pt accumulation in the extracellular matrix.[114]

A recent report aimed at correlating hypoxic regions in tumor tissue with platinum images determined by LA-ICP-MSI in a murine xenograft model after administration of three platinum(IV) compounds (Fig. 2, satraplatin, **3** and **4**). The underlying histology was reflected in the platinum distribution maps. For one tumor section a hypoxic region (visualized by pimonidazole staining) co-localised with a rim of Pt enrichment around the central necrotic region.[73]

A quantitative LA-ICP-MSI setup based on printed patterns as standards and gold layers as pseudo-internal standard has been reported.[108] The method was used to probe intratumoral

Pt distribution in human malignant pleural mesothelioma samples (after treatment with cisplatin), a cancer type that is highly resistant to chemotherapies. The LA-ICP-MSI platinum images were overlayed with the histology (visualized by an haematoxylin eosin stain, Fig. 5B). Platinum concentrations varied more than one order of magnitude over the tumor section, with high Pt localisation in regions where there are no viable tumor cells remaining. In regions with viable tumor cells and blood vessels Pt was not detected. The poor drug tumor penetration of this cancer type is responsible for the resistance to chemotherapy.[108]

LA-ICP-MSI setups have been developed for the study of side effects of platinum-based chemotherapy (*e.g.* nephrotoxicity and ototoxicity). The kidney, which has a complex functionality and histological fine structures, was studied to probe the relationship between cisplatin-induced nephrotoxicity and platinum distribution. LA-ICP-MSI of kidney sections of rats treated with pharmacological doses of cisplatin with a spatial resolution of 8 μm revealed that platinum accumulation was mainly observed in the renal cortex, more specifically in the corticomedullary junction, where the proximal tubules are located (Fig. 6A).[85] A correlation of decreased copper and zinc levels with enhanced platinum accumulation was found which indicates these elements are displaced in renal cells by platinum species. In addition, the nephroprotective function of cilastatin was tested, showing that coadministration results in decreased platinum levels in the cortex.[85] Consecutive LA-ICP-MSI studies on kidney sections following administration with cisplatin showed similar patterns with the cortical localization of platinum predominating.[48,77,79,82] One study showed a platinum concentration gradient from the medulla to the cortex which could be attributed, at least in part, to the treatment regimen as mice were sacrificed only 1 hour after cisplatin administration.[87] LA-ICP-MSI was also used to compare the metal distribution in the kidney upon administration of cisplatin, carboplatin or oxaliplatin as a possible indication for nephrotoxic potential. Following administration of cisplatin, carboplatin or oxaliplatin to rats at clinically relevant doses, kidney sections were analyzed by LA-ICP-MSI and platinum accumulation was observed mainly in the cortical area for cisplatin and carboplatin, whereas for oxaliplatin the platinum distribution

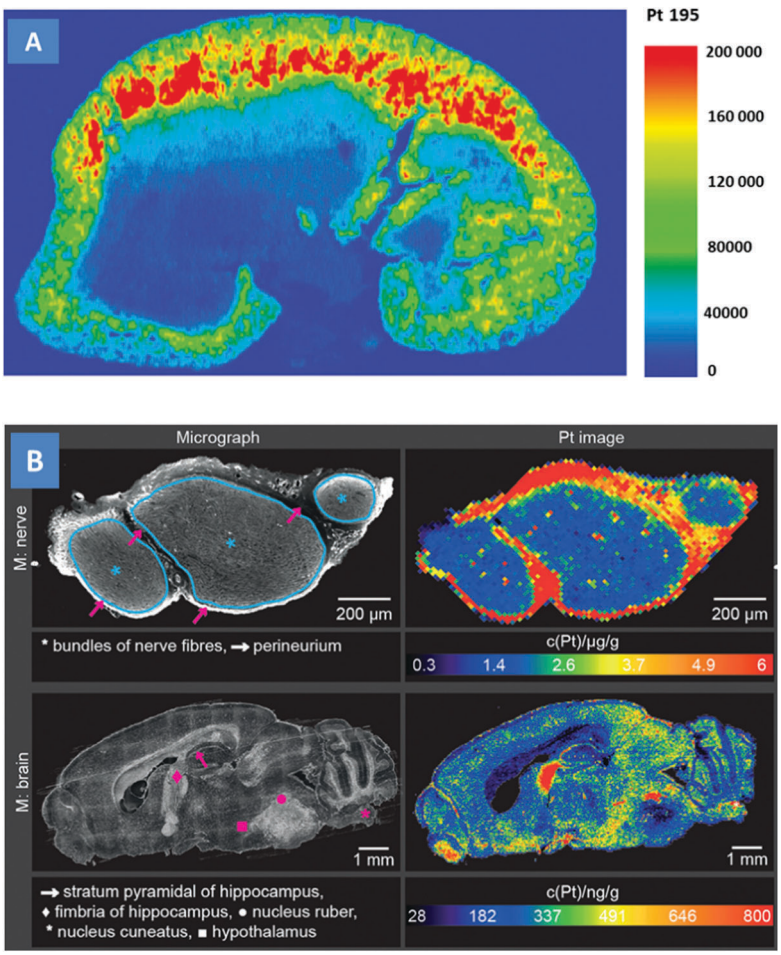

Fig. 6 (A) Platinum distribution in a kidney section after treatment with cisplatin showing predominant Pt localisation in the cortical region (adapted with permission from ref. 85. Copyright 2011 American Chemical Society). (B) Images of sciatic nerve and brain sections from cisplatin-treated mouse. Optical micrograph images (left) and quantitative Pt images (right) determined by LA-ICP-MSI (adapted from ref. 79 with permission from the Royal Society of Chemistry).

appeared to be homogenously distributed along the surface of the ablated kidney section indicating that accumulation also occurs in the medullary region.[77] Notably, these qualitative differences in platinum uptake could be correlated with the different nephrotoxic behaviour of the compounds and the observed accumulation of platinum in the cortex of the kidney is in accordance with the toxicity to proximal tubule cells, located in the cortico-medullary junction. Interestingly, a similar renal metal accumulation pattern as that observed for cisplatin was also observed for the clinically evaluated platinum- and ruthenium-based complexes oxaliplatin, satraplatin and NKP1339, *i.e.* involving elevated metal deposition in the cortex.[48,80] However, in contrast to cisplatin, nephrotoxicity has not been observed as severe side-effect in preclinical or clinical trials for these compounds, possibly due to more efficient elimination with time.

A quantitative LA-ICP-MSI method has been developed based on polymer-embedded standards to elucidate the distribution and retention behaviour of cisplatin in therapy-affected mouse organs (kidney, cochlea and testis). Platinum accumulation was investigated at two time points (1 hour and 4 days). In general, highest platinum levels were found for both time points in areas with a high blood supply, such as in the outer capsule of the testis and the bone areas in the cochlea. After 4 days a 95% decrease of platinum levels was observed in all investigated organs compared to after just 1 hour.

Ototoxicity is another side effect of cisplatin-based chemotherapy with long-term exposure to cisplatin leading to accumulation of platinum in the inner ear and degradation of sensory cells.[82] Another study also used LA-ICP-MSI to locate the platinum in the injured functional structures of toxicity-affected organs during repeated cisplatin treatment (Fig. 6B). The optimal spatial resolution was established for every tissue of interest, based on histological slides, which were correlated with the platinum images. This approach allowed platinum to be detected and quantified in damaged testicles (infertility), cochlea (ototoxicity), kidney (nephrotoxicity) and sciatic nerves, as well as in the brain (neurotoxicity).[79]

One study reported on the combination of direct infusion ICP-MS and LA-ICP-MSI analysis to study the biodistribution and relative bioavailability of two experimental platinum(II) complexes in comparison to cisplatin (Fig. 2, **1** and **2**). LA-ICP-MSI was employed to analyse the platinum deposition in mouse liver and kidney sections with a spatial resolution of $\sim$50 μm. All three platinum complexes accumulated platinum in the cortex region with highest localisation for cisplatin. The amount of platinum accumulation determined by direct infusion ICP-MS and LA-ICP-MSI were found to be in accordance and the platinum uptake was dependent on the lipophilicity and solubility of the complexes.[71]

LA-ICP-MSI was employed to compare the Ru and Pt distributions in different mice tissues (kidney, liver, muscle and spleen) following treatment with KP1339 and cisplatin.[48] A quantitative LA-ICP-MSI bioimaging approach based on matrix-matched calibration standards was developed and validated by microwave digestion and direct infusion ICP-MS. KP1339 exhibited similar metal accumulation patterns to cisplatin in the investigated organs. The metal concentration in organs was higher for KP1339 than for cisplatin, but no histologic alterations were observed which is in accordance with the absence of severe side effects in clinical trials involving KP1339.[48] In a related study on clinical samples, cisplatin and oxaliplatin extravasation was quantified in different tissue types (muscle, nerve tissue, connective tissue and fat tissue), and the platinum burden was correlated with histologic structures and the clinical outcome of the patients.[81]

The potential of LA-ICP-MSI for therapeutic monitoring of platinum in hair of a patient undergoing cisplatin treatment was evaluated in a proof-of-principle study employing a calibration strategy based on Pt-enriched hair strands. The cisplatin-treatment cycle of 3 week intervals was clearly reflected in the spatially-resolved Pt signal of the single hair strand of the patient.[86] LA-ICP-MSI was also employed to study the spatially-resolved platinum distribution in *Caenorhabditis elegans* (an established model organism for biomedical research) upon treatment with cisplatin. The spatial resolution of $\sim$5 μm enabled platinum accumulation to be assigned to the anatomic structures of the model organism with predominant Pt localisation in the intestine and the head of the worms. Cisplatin showed to be uptaken in time and dose dependent manner. The developed laser method for imaging of this model organism could be useful to study cisplatin toxicity and pharmacokinetics.[78]

In metal-based anticancer drug research MALDI-MS has been used to characterise RAPTA–human serum albumin conjugates.[26,112] Bioimaging of metal-based compounds by MALDI-MSI tends to suffer from poor ionization efficiency and signal suppression due to matrix effects of the complexity of biological sample material. To this end, MALDI-TOF-MSI as an imaging tool on the organ level was applied to study the distribution of oxaliplatin and its metabolites in a rat kidney section following HIPEC-like treatment. The developed approach showed that oxaliplatin and its monomethionine and monocysteine complexes localised in the renal cortex.[66] In a recent study, an approach using a derivatization agent, prior to matrix deposition, to increase ionization efficiency of platinum species by MALDI-MSI was described. For the first time oxaliplatin and its metabolites were successfully mapped by MALDI-MSI in multicellular tumor spheroids mimicking HIPEC treatment. Most of the free drug was detected in the outer region while oxaliplatin bound to methionine was found in the core of the spheroids.[65]

Synergies of mass spectrometry imaging techniques

The use of complementary MSI techniques permits different elemental and isotopic/compound distributions to be overlaid. One such study used LA-ICP-MSI in combination with MALDI-MSI.[57] Clinical samples from patients undergoing cisplatin or oxaliplatin chemotherapy against peritoneal carcinosis were analyzed by both imaging techniques to obtain knowledge on the distributions of platinum and platinum-containing molecules, respectively within a single tumor tissue section. For oxaliplatin, the species found by MALDI-MSI was exclusively the monomethionine conjugates of the drug at the periphery of the tumor tissue. Poor drug tumor penetration was also confirmed by LA-ICP-MSI analysis revealing platinum hotspots only on the outside of the

sample. Mapping of cisplatin by LA-ICP-MSI showed the presence of platinum inside the tumor tissue, however no platinum species were detected with MALDI-MSI.[57]

Simultaneous acquisition of MALDI-MSI and LA-ICP-MSI is challenging as different preparation strategies are required and consecutive sections should be analyzed. To overcome this obstacle, LA-ICP-MSI was combined with atmospheric pressure chemical ionisation (APCI)-MS, *i.e.* the laser ablation system is coupled with both ICP-MS and APCI-MS.[83] The instrumental setup allows simultaneous determination of elemental and molecular information from the same sample. As proof-of-principle, the setup was applied to a haematoxylin stained kidney section obtained from a cisplatin-treated mouse. Focused on method development, this study yielded elemental and molecular information for the staining agents eosin and haematoxylin. For cisplatin only Pt images determined by LA-ICP-MSI were obtained.[83]

Recently, LA-ICP-MSI was combined with laser induced breakdown spectroscopy (LIBS) in order to simultaneously map trace, minor and bulk elements in biological tissues.[72] The instrument parameters were adapted for tandem LA-ICP-MSI/LIBS measurements and the optimised setup was applied to a human malignant pleural mesothelioma sample (after treatment with cisplatin) as proof-of-concept. Elemental distribution maps with a spatial resolution of $\sim$40 μm were obtained and correlated with histological features of the tumor tissue. Platinum was found to be mainly accumulated in healthy tissue which was already described earlier for this type of tumor. LIBS appears to be an optimal complementary tool to LA-ICP-MSI for bioimaging experiments. LIBS analysis provides information on major elements which are not accessible *via* ICP-MS (*e.g.* H, O, F) and minor elements (*e.g.* Na, K, Ca, Mg *etc.*) which suffer from high background signals or polyatomic interferences when measuring ICP-MS. In addition, the tandem LA-ICP-MSI/LIBS configuration allows simultaneous data acquisition without the trade-off between spatial resolution and number of analytes measured.[72]

As mentioned in the MSI for cellular imaging section, a multiscale imaging approach based on LA-ICP-MSI and NanoSIMS was recently used to study the distribution of platinum(IV) complexes at tissue and subcellular levels in murine kidney and tumor samples.[59] The sensitivity of NanoSIMS for certain metals is relatively low. Therefore, LA-ICP-MSI was employed to precharacterise platinum accumulation in regions of interest on an organ level. Areas with high platinum content were selected for NanoSIMS experiments to characterise the elemental distribution at subcellular level. This study showed that LA-ICP-MSI and NanoSIMS complement each other in terms of spatial resolution to gain information on metal-based drug distribution on supracellular as well as on subcellular levels.[59]

Conclusions and future directions

Imaging methods that require no modification of the metallodrug, have high sample processing throughput, possess high spatial resolution for resolving small structural features and require minimal sample preparation are desirable. From our review of MSI methods available, careful selection of methods for the desired metallodrug imaging application, whether in cells, tissues or organs, is essential in order to obtain useful and reliable information.

For imaging on a cellular level, the high spatial resolution of NanoSIMS makes the technique ideal for determining metallodrug distribution in different organelles within the cell and ascertain the intracellular ligand state of these drugs via isotopic labelling. Thus far, NanoSIMS has been used to image gold, platinum and ruthenium distributions in cells with a spatial resolution of up to 80 nm. However, some challenges remain, for example sensitivity for certain metals are low and the spatial resolution that can be achieved is insufficient for differentiating smaller cellular structures such as centrioles and ribosomes although this can be partially overcome with the use of correlative electron microscopy. Cell fixation and resin embedding methods used to protect the sample under high vacuum precludes the use of these techniques in live cell imaging and can potentially introduce distributional artifacts. Future developments in ion beam technology such as a recently improved plasma oxygen primary ion source[115,116] and prudent selection of secondary ions based on the metal analyte of interest could provide further improvements in sensitivity and spatial resolution. Furthermore, improvements in sample preparation such as the use of cryo-fixation over traditional chemical fixation[115] or methods that circumvent the need for resin embedding without affecting sample integrity would facilitate the acquisition of reliable imaging data.

Imaging the distribution of metallodrugs in tissue/organs tends to be performed with LA-ICP-MSI due to the high sensitivity for metal detection as well as the high raster rate, a requirement when analyzing large surfaces. In the field of LA-ICP-MSI, the development of low dispersion ablation cells in recent years has significantly improved the throughput for high lateral resolution imaging due to faster wash-out times and better aerosol transport efficiency. However, fast aerosol transport times also require fast ICP-MS measurements. Classical scanning-based ICP-MS restricts the number of isotopes that can be monitored within a transient profile delivered by low dispersion cells. ICP-TOF-MSI, in contrast, offers pseudo-simultaneous detection without a compromise between the transient signal and the number of analytes measured. As many clinical applications demand multi-element information, the combination of low dispersion cells and ICP-TOF-MSI could become an attractive tool for the future for high speed and high resolution imaging in metallodrug research.

Due to current technological limitations MALDI-MSI and TOF-SIMS are less frequently used for metallodrug imaging in biological tissues. However, with further improvements in spatial resolution and sensitivity, these techniques could become useful as they provide molecular information on the metallated species formed and the cellular environment, *i.e.* the distribution of lipids, proteins and sugars, in a single scan. This could greatly enhance our knowledge of the effect of different biological environments on metallodrug behavior.

In the longer term, the imaging methods described in this review together with advances in these techniques could be combined in a systems biology based approach with complementary methods such as genomics, metabolomics and proteomics to provide a molecular level understanding of metal-based drugs on a wide range of cancer types. A unifying approach of this type will provide the gateway to new metal-based drugs by design, rather than the more empirical methods currently employed.

Acknowledgements

We thank the NCCR in Chemical Biology (Swiss National Science Foundation) for funding.

References

1 B. Rosenberg, L. VanCamp and T. Krigas, Inhibition of Cell Division in *Escherichia coli* by Electrolysis Products from a Platinum Electrode, *Nature*, 1965, **205**, 698–699.
2 M. Galanski, V. B. Arion, M. A. Jakupec and B. K. Keppler, Recent developments in the field of tumor-inhibiting metal complexes, *Curr. Pharm. Des.*, 2003, **9**, 2078–2089.
3 N. J. Wheate, S. Walker, G. E. Craig and R. Oun, The status of platinum anticancer drugs in the clinic and in clinical trials, *Dalton Trans.*, 2010, **39**, 8113–8127.
4 C. S. Allardyce and P. J. Dyson, Metal-based drugs that break the rules, *Dalton Trans.*, 2016, **45**, 3201–3209.
5 S. Leijen, S. Burgers, P. Baas, D. Pluim, M. Tibben, E. van Werkhoven, E. Alessio, G. Sava, J. Beijnen and J. M. Schellens, Phase I/II study with ruthenium compound NAMI-A and gemcitabine in patients with non-small cell lung cancer after first line therapy, *Invest. New Drugs*, 2015, **33**, 201–214.
6 N. Graf and S. J. Lippard, Redox activation of metal-based prodrugs as a strategy for drug delivery, *Adv. Drug Delivery Rev.*, 2012, **64**, 993–1004.
7 R. Trondl, P. Heffeter, C. R. Kowol, M. A. Jakupec, W. Berger and B. K. Keppler, NKP-1339, the first ruthenium-based anticancer drug on the edge to clinical application, *Chem. Sci.*, 2014, **5**, 2925–2932.
8 A. Bergamo, C. Gaiddon, J. H. M. Schellens, J. H. Beijnen and G. Sava, Approaching tumour therapy beyond platinum drugs: status of the art and perspectives of ruthenium drug candidates, *J. Inorg. Biochem.*, 2012, **106**, 90–99.
9 L. Messori, G. Marcon and P. Orioli, Gold(III) Compounds as New Family of Anticancer Drugs, *Bioinorg. Chem. Appl.*, 2003, **1**, 177–187.
10 G. Gasser, I. Ott and N. Metzler-Nolte, Organometallic Anticancer Compounds, *J. Med. Chem.*, 2011, **54**, 3–25.
11 http://www.mims.co.uk/drugs/cancer/antineoplastics/cisplatin.
12 http://www.mims.co.uk/drugs/cancer/antineoplastics/oxaliplatin.
13 B. Stordal, N. Pavlakis and R. Davey, Oxaliplatin for the treatment of cisplatin-resistant cancer: a systematic review, *Cancer Treat. Rev.*, 2007, **33**, 347–357.
14 E. Alessio, G. Mestroni, A. Bergamo and G. Sava, Ruthenium Antimetastatic Agents, *Curr. Top. Med. Chem.*, 2004, **4**, 1525–1535.
15 S. Dasari and P. Bernard Tchounwou, Cisplatin in cancer therapy: molecular mechanisms of action, *Eur. J. Pharmacol.*, 2014, **740**, 364–378.
16 C. Scolaro, C. G. Hartinger, C. S. Allardyce, B. K. Keppler and P. J. Dyson, Hydrolysis study of the bifunctional antitumour compound RAPTA-C, [Ru(η6-*p*-cymene)Cl2(pta)], *J. Inorg. Biochem.*, 2008, **102**, 1743–1748.
17 D. J. Hare, E. P. Raven, B. R. Roberts, M. Bogeski, S. D. Portbury, C. A. McLean, C. L. Masters, J. R. Connor, A. I. Bush, P. J. Crouch and P. A. Doble, Laser ablation-inductively coupled plasma-mass spectrometry imaging of white and gray matter iron distribution in Alzheimer's disease frontal cortex, *NeuroImage*, 2016, **137**, 124–131.
18 A.-M. Florea and D. Büsselberg, Cisplatin as an Anti-Tumor Drug: Cellular Mechanisms of Activity, Drug Resistance and Induced Side Effects, *Cancers*, 2011, **3**, 1351–1371.
19 C. Scolaro, A. Bergamo, L. Brescacin, R. Delfino, M. Cocchietto, G. Laurenczy, T. J. Geldbach, G. Sava and P. J. Dyson, *In Vitro* and *In Vivo* Evaluation of Ruthenium(II)–Arene PTA Complexes, *J. Med. Chem.*, 2005, **48**, 4161–4171.
20 S. J. M. Van Malderen, E. Vergucht, M. De Rijcke, C. Janssen, L. Vincze and F. Vanhaecke, Quantitative Determination and Subcellular Imaging of Cu in Single Cells *via* Laser Ablation-ICP-Mass Spectrometry Using High-Density Microarray Gelatin Standards, *Anal. Chem.*, 2016, **88**, 5783–5789.
21 S. J. M. Van Malderen, J. T. van Elteren and F. Vanhaecke, Development of a fast laser ablation-inductively coupled plasma-mass spectrometry cell for sub-μm scanning of layered materials, *J. Anal. At. Spectrom.*, 2015, **30**, 119–125.
22 S. J. M. Van Malderen, J. T. van Elteren and F. Vanhaecke, Submicrometer Imaging by Laser Ablation-Inductively Coupled Plasma Mass Spectrometry via Signal and Image Deconvolution Approaches, *Anal. Chem.*, 2015, **87**, 6125–6132.
23 M. V. Babak, S. M. Meier, K. V. M. Huber, J. Reynisson, A. A. Legin, M. A. Jakupec, A. Roller, A. Stukalov, M. Gridling, K. L. Bennett, J. Colinge, W. Berger, P. J. Dyson, G. Superti-Furga, B. K. Keppler and C. G. Hartinger, Target profiling of an antimetastatic RAPTA agent by chemical proteomics: relevance to the mode of action, *Chem. Sci.*, 2015, **6**, 2449–2456.
24 J. Sabine Becker, Imaging of metals in biological tissue by laser ablation inductively coupled plasma mass spectrometry (LA-ICP-MS): state of the art and future developments, *J. Mass Spectrom.*, 2013, **48**, 255–268.
25 J. L. Norris and R. M. Caprioli, Analysis of Tissue Specimens by Matrix-Assisted Laser Desorption/Ionization Imaging Mass Spectrometry in Biological and Clinical Research, *Chem. Rev.*, 2013, **113**, 2309–2342.
26 I. N. Stepanenko, A. Casini, F. Edafe, M. S. Novak, V. B. Arion, P. J. Dyson, M. A. Jakupec and B. K. Keppler, Conjugation of Organoruthenium(II) 3-(1*H*-Benzimidazol-2-yl)pyrazolo[3,4-*b*]pyridines and Indolo[3,2-*d*]benzazepines to

Recombinant Human Serum Albumin: a Strategy To Enhance Cytotoxicity in Cancer Cells, *Inorg. Chem.*, 2011, **50**, 12669–12679.

27 J. S. Becker, A. Matusch and B. Wu, Bioimaging mass spectrometry of trace elements – recent advance and applications of LA-ICP-MS: a review, *Anal. Chim. Acta*, 2014, **835**, 1–18.

28 L. Wedlock and S. J. Berners-Price, Recent Advances in Mapping the Sub-cellular Distribution of Metal-Based Anticancer Drugs, *Aust. J. Chem.*, 2011, **64**, 692–704.

29 Z. Qin, J. A. Caruso, B. Lai, A. Matusch and J. S. Becker, Trace metal imaging with high spatial resolution: applications in biomedicine, *Metallomics*, 2011, **3**, 28–37.

30 M. L. Pacholski and N. Winograd, Imaging with Mass Spectrometry, *Chem. Rev.*, 1999, **99**, 2977–3006.

31 P. Hoppe, S. Cohen and A. Meibom, NanoSIMS: Technical Aspects and Applications in Cosmochemistry and Biological Geochemistry, *Geostand. Geoanal. Res.*, 2013, **37**, 111–154.

32 C. R. M. Grovenor, K. E. Smart, M. Kilburn, J. R. Dilworth, B. Martin, C. Hawes and R. E. M. Rickaby, Specimen preparation for NanoSIMS analysis of biological materials, *Appl. Surf. Sci.*, 2006, **252**, 6917–6924.

33 F. Benabdellah, A. Seyer, L. Quinton, D. Touboul, A. Brunelle and O. Laprévote, Mass spectrometry imaging of rat brain sections: nanomolar sensitivity with MALDI *versus* nanometer resolution by TOF-SIMS, *Anal. Bioanal. Chem.*, 2010, **396**, 151–162.

34 A. A. Gulin, M. S. Pavlyukov, S. K. Gularyan and V. A. Nadtochenko, Visualization of the spatial distribution of Pt+ ions in cisplatin-treated glioblastoma cells by time-of-flight secondary ion mass spectrometry, *Biochemistry*, 2015, **9**, 202–209.

35 J.-L. Guerquin-Kern, T.-D. Wu, C. Quintana and A. Croisy, Progress in analytical imaging of the cell by dynamic secondary ion mass spectrometry (SIMS microscopy), *Biochim. Biophys. Acta, Gen. Subj.*, 2005, **1724**, 228–238.

36 J. S. Fletcher, Cellular imaging with secondary ion mass spectrometry, *Analyst*, 2009, **134**, 2204–2215.

37 B. Gammelgaard, S. Stürup and C. Møller, in *Encyclopedia of Drug Metabolism and Interactions*, ed. A. V. Lyubimov, John Wiley & Sons, Inc., 2011.

38 E. E. M. Brouwers, M. Tibben, H. Rosing, J. H. M. Schellen and J. H. Beijnen, The application of inductively coupled plasma mass spectrometry in clinical pharmacological oncology research, *Mass Spectrom. Rev.*, 2008, **27**, 67–100.

39 A. R. Timerbaev, Recent progress of ICP-MS in the development of metal-based drugs and diagnostic agents, *J. Anal. At. Spectrom.*, 2014, **29**, 1058–1072.

40 H. Holtkamp, G. Grabmann and C. G. Hartinger, Electrophoretic separation techniques and their hyphenation to mass spectrometry in biological inorganic chemistry, *Electrophoresis*, 2016, **37**, 959–972.

41 J. S. Becker, M. Zoriy, A. Matusch, B. Wu, D. Salber, C. Palm and J. S. Becker, Bioimaging of metals by laser ablation inductively coupled plasma mass spectrometry (LA-ICP-MS), *Mass Spectrom. Rev.*, 2010, **29**, 156–175.

42 J. S. Becker and N. Jakubowski, The synergy of elemental and biomolecular mass spectrometry: new analytical strategies in life sciences, *Chem. Soc. Rev.*, 2009, **38**, 1969–1983.

43 D. Pozebon, G. L. Scheffler, V. L. Dressler and M. A. G. Nunes, Review of the applications of laser ablation inductively coupled plasma mass spectrometry (LA-ICP-MS) to the analysis of biological samples, *J. Anal. At. Spectrom.*, 2014, **29**, 2204–2228.

44 S. J. M. Van Malderen, A. J. Managh, B. L. Sharp and F. Vanhaecke, Recent developments in the design of rapid response cells for laser ablation-inductively coupled plasma-mass spectrometry and their impact on bioimaging applications, *J. Anal. At. Spectrom.*, 2016, **31**, 423–439.

45 A. Gundlach-Graham and D. Günther, Toward faster and higher resolution LA-ICPMS imaging: on the co-evolution of LA cell design and ICPMS instrumentation, *Anal. Bioanal. Chem.*, 2016, **408**, 2687–2695.

46 I. Konz, B. Fernández, M. Fernández, R. Pereiro and A. Sanz-Medel, Laser ablation ICP-MS for quantitative biomedical applications, *Anal. Bioanal. Chem.*, 2012, **403**, 2113–2125.

47 D. Hare, C. Austin and P. Doble, Quantification strategies for elemental imaging of biological samples using laser ablation-inductively coupled plasma-mass spectrometry, *Analyst*, 2012, **137**, 1527–1537.

48 A. E. Egger, S. Theiner, C. Kornauth, P. Heffeter, W. Berger, B. K. Keppler and C. Hartinger, Quantitative bioimaging by LA-ICP-MS: a methodological study on the distribution of Pt and Ru in viscera originating from cisplatin- and KP1339-treated mice, *Metallomics*, 2014, **6**, 1616–1625.

49 A. Limbeck, P. Galler, M. Bonta, G. Bauer, W. Nischkauer and F. Vanhaecke, Recent advances in quantitative LA-ICP-MS analysis: challenges and solutions in the life sciences and environmental chemistry, *Anal. Bioanal. Chem.*, 2015, **407**, 6593–6617.

50 D. A. Frick and D. Gunther, Fundamental studies on the ablation behaviour of carbon in LA-ICP-MS with respect to the suitability as internal standard, *J. Anal. At. Spectrom.*, 2012, **27**, 1294–1303.

51 C. Austin, F. Fryer, J. Lear, D. Bishop, D. Hare, T. Rawling, L. Kirkup, A. McDonagh and P. Doble, Factors affecting internal standard selection for quantitative elemental bioimaging of soft tissues by LA-ICP-MS, *J. Anal. At. Spectrom.*, 2011, **26**, 1494–1501.

52 I. Konz, B. Fernández, M. L. Fernández, R. Pereiro, H. González, L. Álvarez, M. Coca-Prados and A. Sanz-Medel, Gold internal standard correction for elemental imaging of soft tissue sections by LA-ICP-MS: element distribution in eye microstructures, *Anal. Bioanal. Chem.*, 2013, **405**, 3091–3096.

53 M. Bonta, H. Lohninger, M. Marchetti-Deschmann and A. Limbeck, Application of gold thin-films for internal standardization in LA-ICP-MS imaging experiments, *Analyst*, 2014, **139**, 1521–1531.

54 L. F. Marvin, M. A. Roberts and L. B. Fay, Matrix-assisted laser desorption/ionization time-of-flight mass spectrometry in clinical chemistry, *Clin. Chim. Acta*, 2003, **337**, 11–21.

55 M. Aichler and A. Walch, MALDI Imaging mass spectrometry: current frontiers and perspectives in pathology research and practice, *Lab. Invest.*, 2015, **95**, 422–431.
56 B. Li, S. J. B. Dunham, Y. Dong, S. Yoon, M. Zeng and J. V. Sweedler, Analytical capabilities of mass spectrometry imaging and its potential applications in food science, *Trends Food Sci. Technol.*, 2016, **47**, 50–63.
57 J. Bianga, A. Bouslimani, N. Bec, F. Quenet, S. Mounicou, J. Szpunar, B. Bouyssiere, R. Lobinski and C. Larroque, Complementarity of MALDI and LA ICP mass spectrometry for platinum anticancer imaging in human tumor, *Metallomics*, 2014, **6**, 1382–1386.
58 M. T. Proetto, C. R. Anderton, D. Hu, C. J. Szymanski, Z. Zhu, J. P. Patterson, J. K. Kammeyer, L. G. Nilewski, A. M. Rush, N. C. Bell, J. E. Evans, G. Orr, S. B. Howell and N. C. Gianneschi, Cellular Delivery of Nanoparticles Revealed with Combined Optical and Isotopic Nanoscopy, *ACS Nano*, 2016, **10**, 4046–4054.
59 A. A. Legin, S. Theiner, A. Schintlmeister, S. Reipert, P. Heffeter, M. A. Jakupec, J. Mayr, H. P. Varbanov, C. R. Kowol, M. Galanski, W. Berger, M. Wagner and B. K. Keppler, Multi-scale imaging of anticancer platinum(IV) compounds in murine tumor and kidney, *Chem. Sci.*, 2016, **7**, 3052–3061.
60 R. F. S. Lee, S. Escrig, M. Croisier, S. Clerc-Rosset, G. W. Knott, A. Meibom, C. A. Davey, K. Johnsson and P. J. Dyson, NanoSIMS analysis of an isotopically labelled organometallic ruthenium(II) drug to probe its distribution and state *in vitro*, *Chem. Commun.*, 2015, **51**, 16486–16489.
61 A. A. Legin, A. Schintlmeister, M. A. Jakupec, M. Galanski, I. Lichtscheidl, M. Wagner and B. K. Keppler, NanoSIMS combined with fluorescence microscopy as a tool for subcellular imaging of isotopically labeled platinum-based anticancer drugs, *Chem. Sci.*, 2014, **5**, 3135–3143.
62 L. E. Wedlock, M. R. Kilburn, R. Liu, J. A. Shaw, S. J. Berners-Price and N. P. Farrell, NanoSIMS multi-element imaging reveals internalisation and nucleolar targeting for a highly-charged polynuclear platinum compound, *Chem. Commun.*, 2013, **49**, 6944–6946.
63 L. E. Wedlock, M. R. Kilburn, J. B. Cliff, L. Filgueira, M. Saunders and S. J. Berners-Price, , Visualising gold inside tumour cells following treatment with an anti-tumour gold(I) complex, *Metallomics*, 2011, **3**, 917–925.
64 S. Chandra, in *Mass Spectrometry Imaging: Principles and Protocols*, ed. S. S. Rubakhin and V. J. Sweedler, Humana Press, Totowa, NJ, 2010, pp. 113–130.
65 X. Liu and A. B. Hummon, Chemical Imaging of Platinum-Based Drugs and their Metabolites, *Sci. Rep.*, 2016, **6**, 38507.
66 A. Bouslimani, N. Bec, M. Glueckmann, C. Hirtz and C. Larroque, Matrix-assisted laser desorption/ionization imaging mass spectrometry of oxaliplatin derivatives in heated intraoperative chemotherapy (HIPEC)-like treated rat kidney, *Rapid Commun. Mass Spectrom.*, 2010, **24**, 415–421.
67 E. Moreno-Gordaliza, D. Esteban-Fernandez, C. Giesen, K. Lehmann, A. Lazaro, A. Tejedor, C. Scheler, B. Canas, N. Jakubowski, M. W. Linscheid and M. M. Gomez-Gomez, LA-ICP-MS and nHPLC-ESI-LTQ-FT-MS/MS for the analysis of cisplatin-protein complexes separated by two dimensional gel electrophoresis in biological samples, *J. Anal. At. Spectrom.*, 2012, **27**, 1474–1483.
68 I. Khalaila, A. Bergamo, F. Bussy, G. Sava and P. J. Dyson, The role of cisplatin and NAMI-A plasma–protein interactions in relation to combination therapy, *Int. J. Oncol.*, 2006, **29**, 261–268.
69 C. S. Allardyce, P. J. Dyson, F. R. Abou-Shakra, H. Birtwistle and J. Coffey, Inductively coupled plasma mass spectrometry to identify protein drug targets from whole cell systems, *Chem. Commun.*, 2001, 2708–2709.
70 T. Van Acker, S. J. M. Van Malderen, M. Van Heerden, J. E. McDuffie, F. Cuyckens and F. Vanhaecke, High-resolution laser ablation-inductively coupled plasma-mass spectrometry imaging of cisplatin-induced nephrotoxic side effects, *Anal. Chim. Acta*, 2016, **945**, 23–30.
71 T.-S. Lum, C.-L. Ho, Y.-K. Tsoi, C.-H. Siu, P. Y.-K. Yue, W.-Y. Wong and K. S.-Y. Leung, Elemental bioimaging of platinum in mouse tissues by laser ablation-inductively coupled plasma-mass spectrometry for the study of localization behavior of structurally similar complexes, *Int. J. Mass Spectrom.*, 2016, **404**, 40–47.
72 M. Bonta, J. J. Gonzalez, C. D. Quarles, R. E. Russo, B. Hegedus and A. Limbeck, Elemental mapping of biological samples by the combined use of LIBS and LA-ICP-MS, *J. Anal. At. Spectrom.*, 2016, **31**, 252–258.
73 E. Schreiber-Brynzak, V. Pichler, P. Heffeter, B. Hanson, S. Theiner, I. Lichtscheidl-Schultz, C. Kornauth, L. Bamonti, V. Dhery, D. Groza, D. Berry, W. Berger, M. Galanski, M. A. Jakupec and B. K. Keppler, Behavior of platinum(IV) complexes in models of tumor hypoxia: cytotoxicity, compound distribution and accumulation, *Metallomics*, 2016, **8**, 422–433.
74 S. Theiner, E. Schreiber-Brynzak, M. A. Jakupec, M. Galanski, G. Koellensperger and B. K. Keppler, LA-ICP-MS imaging in multicellular tumor spheroids – a novel tool in the preclinical development of metal-based anticancer drugs, *Metallomics*, 2016, **8**, 398–402.
75 G. K. Gransbury, P. Kappen, C. J. Glover, J. N. Hughes, A. Levina, P. A. Lay, I. F. Musgrave and H. H. Harris, Comparison of KP1019 and NAMI-A in tumour-mimetic environments, *Metallomics*, 2016, **8**, 762–773.
76 A.-C. Niehoff, J. Grünebaum, A. Moosmann, D. Mulac, J. Söbbing, R. Niehaus, R. Buchholz, S. Kröger, A. Wiehe, S. Wagner, M. Sperling, H. von Briesen, K. Langer and U. Karst, Quantitative bioimaging of platinum group elements in tumor spheroids, *Anal. Chim. Acta*, 2016, **938**, 106–113.
77 I. Moraleja, D. Esteban-Fernández, A. Lázaro, B. Humanes, B. Neumann, A. Tejedor, M. L. Mena, N. Jakubowski and M. M. Gómez-Gómez, Printing metal-spiked inks for LA-ICP-MS bioimaging internal standardization: comparison of the different nephrotoxic behavior of cisplatin, carboplatin, and oxaliplatin, *Anal. Bioanal. Chem.*, 2016, 1–10.

78 B. Crone, M. Aschner, T. Schwerdtle, U. Karst and J. Bornhorst, Elemental bioimaging of Cisplatin in Caenorhabditis elegans by LA-ICP-MS, *Metallomics*, 2015, **7**, 1189–1195.
79 C. Koppen, O. Reifschneider, I. Castanheira, M. Sperling, U. Karst and G. Ciarimboli, Quantitative imaging of platinum based on laser ablation-inductively coupled plasma-mass spectrometry to investigate toxic side effects of cisplatin, *Metallomics*, 2015, **7**, 1595–1603.
80 S. Theiner, C. Kornauth, H. P. Varbanov, M. Galanski, S. Van Schoonhoven, P. Heffeter, W. Berger, A. E. Egger and B. K. Keppler, Tumor microenvironment in focus: LA-ICP-MS bioimaging of a preclinical tumor model upon treatment with platinum(IV)-based anticancer agents, *Metallomics*, 2015, **7**, 1256–1264.
81 A. E. Egger, C. Kornauth, W. Haslik, S. Hann, S. Theiner, G. Bayer, C. G. Hartinger, B. K. Keppler, U. Pluschnig and R. M. Mader, Extravasation of Pt-based chemotherapeutics – bioimaging of their distribution in resectates using laser ablation-inductively coupled plasma-mass spectrometry (LA-ICP-MS), *Metallomics*, 2015, **7**, 508–515.
82 O. Reifschneider, C. A. Wehe, I. Raj, J. Ehmcke, G. Ciarimboli, M. Sperling and U. Karst, Quantitative Bioimaging of Platinum in Polymer Embedded Mouse Organs by Laser Ablation ICP-MS, *Metallomics*, 2013, **5**, 1440–1447.
83 C. Herdering, C. A. Wehe, O. Reifschneider, I. Raj, G. Ciarimboli, K. Diebold, C. Becker, M. Sperling and U. Karst, Laser ablation based bioimaging with simultaneous elemental and molecular mass spectrometry: towards spatially resolved speciation analysis, *Rapid Commun. Mass Spectrom.*, 2013, **27**, 2588–2594.
84 D. Gholap, J. Verhulst, W. Ceelen and F. Vanhaecke, Use of pneumatic nebulization and laser ablation–inductively coupled plasma–mass spectrometry to study the distribution and bioavailability of an intraperitoneally administered Pt-containing chemotherapeutic drug, *Anal. Bioanal. Chem.*, 2012, **402**, 2121–2129.
85 E. Moreno-Gordaliza, C. Giesen, A. Lázaro, D. Esteban-Fernández, B. Humanes, B. Cañas, U. Panne, A. Tejedor, N. Jakubowski and M. M. Gómez-Gómez, Elemental Bioimaging in Kidney by LA-ICP-MS As a Tool to Study Nephrotoxicity and Renal Protective Strategies in Cisplatin Therapies, *Anal. Chem.*, 2011, **83**, 7933–7940.
86 D. Pozebon, V. L. Dressler, A. Matusch and J. S. Becker, Monitoring of platinum in a single hair by laser ablation inductively coupled plasma mass spectrometry (LA-ICP-MS) after cisplatin treatment for cancer, *Int. J. Mass Spectrom.*, 2008, **272**, 57–62.
87 M. Zoriy, A. Matusch, T. Spruss and J. S. Becker, Laser ablation inductively coupled plasma mass spectrometry for imaging of copper, zinc, and platinum in thin sections of a kidney from a mouse treated with cis-platin, *Int. J. Mass Spectrom.*, 2007, **260**, 102–106.
88 X. Duan, C. He, S. J. Kron and W. Lin, Nanoparticle formulations of cisplatin for cancer therapy, *Wiley Interdiscip. Rev.: Nanomed. Nanobiotechnol.*, 2016, **8**, 776–791.
89 I. Ott, On the medicinal chemistry of gold complexes as anticancer drugs, *Coord. Chem. Rev.*, 2009, **253**, 1670–1681.
90 S. H. van Rijt and P. J. Sadler, Current applications and future potential for bioinorganic chemistry in the development of anticancer drugs, *Drug Discovery Today*, 2009, **14**, 1089–1097.
91 C. G. Hartinger, N. Metzler-Nolte and P. J. Dyson, Challenges and Opportunities in the Development of Organometallic Anticancer Drugs, *Organometallics*, 2012, **31**, 5677–5685.
92 A. Bindoli, M. P. Rigobello, G. Scutari, C. Gabbiani, A. Casini and L. Messori, Thioredoxin reductase: a target for gold compounds acting as potential anticancer drugs, *Coord. Chem. Rev.*, 2009, **253**, 1692–1707.
93 B. S. Murray, M. V. Babak, C. G. Hartinger and P. J. Dyson, The development of RAPTA compounds for the treatment of tumors, *Coord. Chem. Rev.*, 2016, **306**, 86–114.
94 G. Sava, S. Zorzet, C. Turrin, F. Vita, M. Soranzo, G. Zabucchi, M. Cocchietto, A. Bergamo, S. DiGiovine, G. Pezzoni, L. Sartor and S. Garbisa, Dual Action of NAMI-A in Inhibition of Solid Tumor Metastasis: Selective Targeting of Metastatic Cells and Binding to Collagen, *Clin. Cancer Res.*, 2003, **9**, 1898–1905.
95 Z. Adhireksan, G. E. Davey, P. Campomanes, M. Groessl, C. M. Clavel, H. Yu, A. A. Nazarov, C. H. F. Yeo, W. H. Ang, P. Dröge, U. Rothlisberger, P. J. Dyson and C. A. Davey, Ligand substitutions between ruthenium–cymene compounds can control protein versus DNA targeting and anticancer activity, *Nat. Commun.*, 2014, **5**, 3462.
96 T. C. de Bang and S. Husted, Lanthanide elements as labels for multiplexed and targeted analysis of proteins, DNA and RNA using inductively-coupled plasma mass spectrometry, *TrAC, Trends Anal. Chem.*, 2015, **72**, 45–52.
97 A. Dorcier, P. J. Dyson, C. Gossens, U. Rothlisberger, R. Scopelliti and I. Tavernelli, Binding of Organometallic Ruthenium(II) and Osmium(II) Complexes to an Oligonucleotide: A Combined Mass Spectrometric and Theoretical Study, *Organometallics*, 2005, **24**, 2114–2123.
98 L. Mueller, H. Traub, N. Jakubowski, D. Drescher, V. Baranov and J. Kneipp, Trends in single-cell analysis by use of ICP-MS, *Anal. Bioanal. Chem.*, 2014, **406**, 6963–6977.
99 H. A. O. Wang, D. Grolimund, C. Giesen, C. N. Borca, J. R. H. Shaw-Stewart, B. Bodenmiller and D. Günther, Fast Chemical Imaging at High Spatial Resolution by Laser Ablation Inductively Coupled Plasma Mass Spectrometry, *Anal. Chem.*, 2013, **85**, 10107–10116.
100 C. Giesen, L. Waentig, T. Mairinger, D. Drescher, J. Kneipp, P. H. Roos, U. Panne and N. Jakubowski, Iodine as an elemental marker for imaging of single cells and tissue sections by laser ablation inductively coupled plasma mass spectrometry, *J. Anal. At. Spectrom.*, 2011, **26**, 2160–2165.
101 C. Giesen, T. Mairinger, L. Khoury, L. Waentig, N. Jakubowski and U. Panne, Multiplexed Immunohistochemical Detection of Tumor Markers in Breast Cancer Tissue Using Laser Ablation Inductively Coupled Plasma Mass Spectrometry, *Anal. Chem.*, 2011, **83**, 8177–8183.
102 D. Drescher, C. Giesen, H. Traub, U. Panne, J. Kneipp and N. Jakubowski, Quantitative imaging of gold and silver nanoparticles in single eukaryotic cells by LA-ICP-MS, *Anal. Chem.*, 2012, **84**, 9684–9688.

103 R. A. Alderden, H. R. Mellor, S. Modok, M. D. Hall, S. R. Sutton, M. G. Newville, R. Callaghan and T. W. Hambley, Elemental Tomography of Cancer-Cell Spheroids Reveals Incomplete Uptake of Both Platinum(II) and Platinum(IV) Complexes, *J. Am. Chem. Soc.*, 2007, **129**, 13400–13401.

104 J. Z. Zhang, N. S. Bryce, A. Lanzirotti, C. K. J. Chen, D. Paterson, M. D. de Jonge, D. L. Howard and T. W. Hambley, Getting to the core of platinum drug bio-distributions: the penetration of anti-cancer platinum complexes into spheroid tumour models, *Metallomics*, 2012, **4**, 1209–1217.

105 A. V. Klein and T. W. Hambley, Platinum Drug Distribution in Cancer Cells and Tumors, *Chem. Rev.*, 2009, **109**, 4911–4920.

106 G. Mehta, A. Y. Hsiao, M. Ingram, G. D. Luker and S. Takayama, Opportunities and challenges for use of tumor spheroids as models to test drug delivery and efficacy, *J. Controlled Release*, 2012, **164**, 192–204.

107 F. Hirschhaeuser, H. Menne, C. Dittfeld, J. West, W. Mueller-Klieser and L. A. Kunz-Schughart, Multicellular tumor spheroids: an underestimated tool is catching up again, *J. Biotechnol.*, 2010, **148**, 3–15.

108 M. Bonta, H. Lohninger, V. Laszlo, B. Hegedus and A. Limbeck, Quantitative LA-ICP-MS imaging of platinum in chemotherapy treated human malignant pleural mesothelioma samples using printed patterns as standard, *J. Anal. At. Spectrom.*, 2014, **29**, 2159–2167.

109 C. S. Allardyce, P. J. Dyson, D. J. Ellis, P. A. Salter and R. Scopelliti, Synthesis and characterisation of some water soluble ruthenium(II)–arene complexes and an investigation of their antibiotic and antiviral properties, *J. Organomet. Chem.*, 2003, **668**, 35–42.

110 F. Guidi, I. Landini, M. Puglia, F. Magherini, C. Gabbiani, M. A. Cinellu, S. Nobili, T. Fiaschi, L. Bini, E. Mini, L. Messori and A. Modesti, Proteomic analysis of ovarian cancer cell responses to cytotoxic gold compounds, *Metallomics*, 2012, **4**, 307–314.

111 D. A. Wolters, M. Stefanopoulou, P. J. Dyson and M. Groessl, Combination of metallomics and proteomics to study the effects of the metallodrug RAPTA-T on human cancer cells, *Metallomics*, 2012, **4**, 1185–1196.

112 W. H. Ang, E. Daldini, L. Juillerat-Jeanneret and P. J. Dyson, Strategy To Tether Organometallic Ruthenium–Arene Anticancer Compounds to Recombinant Human Serum Albumin, *Inorg. Chem.*, 2007, **46**, 9048–9050.

113 G. Chiara, M. Francesca, M. Alessandra and M. Luigi, Proteomic and Metallomic Strategies for Understanding the Mode of Action of Anticancer Metallodrugs, *Anti-Cancer Agents Med. Chem.*, 2010, **10**, 324–337.

114 C. Carlier, B. Laforce, S. J. M. Van Malderen, F. Gremonprez, R. Tucoulou, J. Villanova, O. De Wever, L. Vincze, F. Vanhaecke and W. Ceelen, Nanoscopic tumor tissue distribution of platinum after intraperitoneal administration in a xenograft model of ovarian cancer, *J. Pharm. Biomed. Anal.*, 2016, **131**, 256–262.

115 K. L. Moore, E. Lombi, F.-J. Zhao and C. R. M. Grovenor, Elemental imaging at the nanoscale: NanoSIMS and complementary techniques for element localisation in plants, *Anal. Bioanal. Chem.*, 2012, **402**, 3263–3273.

116 J. Malherbe, F. Penen, M.-P. Isaure, J. Frank, G. Hause, D. Dobritzsch, E. Gontier, F. Horréard, F. Hillion and D. Schaumlöffel, A New Radio Frequency Plasma Oxygen Primary Ion Source on Nano Secondary Ion Mass Spectrometry for Improved Lateral Resolution and Detection of Electropositive Elements at Single Cell Level, *Anal. Chem.*, 2016, **88**, 7130–7136.